A&A 658, A80 (2022)
https://doi.org/10.1051/0004-6361/202142234

Astronomy & Astrophysics

Gaia-ESO Survey: Detailed elemental abundances in red giants of the peculiar globular cluster NGC 1851★,★★

G. Tautvaišienė[1], A. Drazdauskas[1], A. Bragaglia[2], S. L. Martell[3,4], E. Pancino[5,6], C. Lardo[7], Š. Mikolaitis[1], R. Minkevičiūtė[1], E. Stonkutė[1], M. Ambrosch[1], V. Bagdonas[1], Y. Chorniy[1], N. Sanna[5], E. Franciosini[5], R. Smiljanic[8], S. Randich[5], G. Gilmore[9], T. Bensby[10], M. Bergemann[11], A. Gonneau[9], G. Guiglion[12], G. Carraro[13], U. Heiter[14], A. Korn[14], L. Magrini[5], L. Morbidelli[5], and S. Zaggia[15]

(Affiliations can be found after the references)

Received 16 September 2021 / Accepted 10 November 2021

ABSTRACT

Context. NGC 1851 is one of several globular clusters for which multiple stellar populations of the subgiant branch have been clearly identified and a difference in metallicity detected. A crucial piece of information on the formation history of this cluster can be provided by the sum of A(C+N+O) abundances. However, these values have lacked a general consensus thus far. The separation of the subgiant branch can be based on age and/or A(C+N+O) abundance differences.

Aims. Our main aim was to determine carbon, nitrogen, and oxygen abundances for evolved giants in the globular cluster NGC 1851 in order to check whether or not the double populations of stars are coeval.

Methods. High-resolution spectra, observed with the FLAMES-UVES spectrograph on the ESO VLT telescope, were analysed using a differential model atmosphere method. Abundances of carbon were derived using spectral synthesis of the C_2 band heads at 5135 and 5635.5 Å. The wavelength interval 6470−6490 Å, with CN features, was analysed to determine nitrogen abundances. Oxygen abundances were determined from the [O I] line at 6300 Å. Abundances of other chemical elements were determined from equivalent widths or spectral syntheses of unblended spectral lines.

Results. We provide abundances of up to 29 chemical elements for a sample of 45 giants in NGC 1851. The investigated stars can be separated into two populations with a difference of 0.07 dex in the mean metallicity, 0.3 dex in the mean C/N, and 0.35 dex in the mean *s*-process dominated element-to-iron abundance ratios [*s*/Fe]. No significant difference was determined in the mean values of A(C+N+O) as well as in abundance to iron ratios of carbon, α- and iron-peak-elements, and of europium.

Conclusions. As the averaged A(C+N+O) values between the two populations do not differ, additional evidence is given that NGC 1851 is composed of two clusters, the metal-rich cluster being by about 0.6 Gyr older than the metal-poor one. A global overview of NGC 1851 properties and the detailed abundances of chemical elements favour its formation in a dwarf spheroidal galaxy that was accreted by the Milky Way.

Key words. stars: abundances – stars: evolution – globular clusters: individual: NGC 1851

1. Introduction

Chemical abundances are an excellent tool for studying the star-formation and self-enrichment histories of Galactic globular clusters. They trace the integrated nucleosynthetic history of the material in the stars: the early supernovae that raised their overall abundance levels into the typical range for globular clusters, the stellar-mode feedback that imprinted the light-element anticorrelations found in every Galactic globular cluster, and the internal processing that marks specific stages of stellar evolution.

Different elements participate in these processes through different nucleosynthetic channels. The iron-peak and α-elements are produced in the early supernovae. The heavy neutron-capture elements are produced in supernovae, in asymptotic giant branch stars, and during mergers of neutron stars and black holes. The light elements from lithium to silicon are produced and destroyed in proton-capture reactions at temperatures typically found in stellar interiors, meaning that their abundance in a star will be a result of stellar feedback into the interstellar medium before it formed as well as the first dredge-up and deep mixing during its lifetime.

The CNO, NeNa, and MgAl cycles, operating in equilibrium, produce anticorrelations in elemental abundances because of the different timescales of the different proton-capture reactions. Carbon, oxygen, and magnesium are depleted, while nitrogen, sodium, and aluminium are produced. This is the same pattern that is observed within globular clusters, which is why it is presumed that globular cluster abundance anomalies could be a result of chemical feedback between multiple generations of star formation early in the history of globular clusters (see reviews by Bastian & Lardo 2018; Gratton et al. 2019).

An intriguing field of research was opened up thanks to the discovery that some globular clusters have stellar populations that differ in metallicity and abundances of slow neutron-capture process (*s*-process) elements (e.g. Carretta et al. 2010; Marino et al. 2011; Lardo et al. 2013; Mucciarelli et al. 2015; Lee 2016; Kovalev et al. 2019, and references therein). These discoveries imply that those clusters must have had a more complex formation history than "normal" globular clusters and may even

★ Full Table 3 is only available at the CDS via anonymous ftp to cdsarc.u-strasbg.fr (130.79.128.5) or via http://cdsarc.u-strasbg.fr/viz-bin/cat/J/A+A/658/A80

★★ Based on data products from observations made with ESO Telescopes at the La Silla Paranal Observatory under programme ID 188.B-3002 (The *Gaia*-ESO Public Spectroscopic Survey, PIs G. Gilmore and S. Randich).

have originated as nuclear star clusters within dwarf galaxies that were captured by the Milky Way in the past (e.g. Bekki & Yong 2012; Massari et al. 2019).

Since the CNO, NeNa, and MgAl cycles operate at successively higher temperatures, they are not always well-coupled in a particular cluster. The CNO cycle is the most universal, since it requires the lowest temperature, while the MgAl cycle and the production of Si through the reaction of ^{27}Al$(p,\gamma)^{28}$Si (see Yong et al. 2005; Ventura et al. 2011 for observational and theoretical discussion of this phenomenon) is only sporadically found in globular clusters. As an example, the range of [Mg/Fe] variation in NGC 6752 is quite small, even though the O-Na anticorrelation is clear (Yong & Grundahl 2008). Pancino et al. (2017a) demonstrated that the extent of the Mg-Al anticorrelation depends on both the mass and metallicity of globular clusters. However, the entire range of anticorrelation behaviour is not well understood because the full abundance pattern from carbon through aluminium is very rarely reported in a single study. This might be due to a technicality: O, Na, Mg, and Al abundances are always derived from resonance lines in high-resolution spectra, while C and N abundances are often derived from molecular features in low-resolution spectra.

Interpretations of carbon and nitrogen abundances can be further complicated by the fact that they can change during a star's lifetime due to internal processes. The first dredge-up is a short-lived phase that occurs shortly after a star has ended core hydrogen burning and begun to transit onto the red giant branch (RGB). During the first dredge-up, a star's convective envelope temporarily expands, spreading into regions that have undergone nuclear burning and then retreating outward. Because the mixing timescale of the convective envelope is quite short, this episode homogenises all material within the envelope, causing the surface abundances to show signs of having undergone hot hydrogen burning. Specifically, the first dredge-up causes a noticeable decrease in [C/Fe], a comprehensive increase in [N/Fe], and a dramatic reduction in the abundance of lithium and the isotopic ratio ^{12}C/^{13}C.

Deep mixing is a non convective circulation process that begins when an RGB star's hydrogen-burning shell crosses the deepest point reached by the first dredge-up and continues for the entire RGB lifetime of the star. The exact mechanism for deep mixing is not known, and theoretical arguments have been made for: rotational mixing (Sweigart & Mengel 1979; Palacios et al. 2003; Chanamé et al. 2005; Denissenkov et al. 2006), magnetic fields (Hubbard & Dearborn 1980; Busso et al. 2007; Nordhaus et al. 2008; Palmerini et al. 2009), rotation and magnetic fields (Eggenberger et al. 2005), internal gravity waves (Zahn et al. 1997; Denissenkov & Tout 2000), thermohaline mixing (Eggleton et al. 2006, 2008; Charbonnel & Zahn 2007; Cantiello & Langer 2010; Charbonnel & Lagarde 2010), combination of thermohaline mixing and magnetic fields (Busso et al. 2007; Denissenkov et al. 2009), and a combination of thermohaline mixing and rotation (Charbonnel & Lagarde 2010; Lagarde et al. 2012). Thus, when investigating and comparing CNO abundances in evolved stars of globular clusters, the stars ought to be of the same evolutionary stage.

It has been suspected long ago that NGC 1851 is chemically heterogeneous (Hesser et al. 1982; Grundahl & Bruntt 2006). The high-precision photometric study with the *Hubble* Space Telescope by Milone et al. (2008) revealed two distinct subgiant branches in NGC 1851 and made this cluster of particular interest. However, explanations of their origin lack a consensus thus far. Ancient globular clusters are usually thought to host two generations of stars. The first is likely primordial and the second born from the ejecta of a fraction of the stars of the first population. Thus, it was initially thought that this could also be the origin of the two subgiant branches in NGC 1851 (e.g. Pancino et al. 2010). Alternatively, there were suggestions that NGC 1851 originated via the merging of two globular clusters (e.g. Campbell et al. 2012) or is a naked nucleus of a captured and disrupted dwarf galaxy (e.g. Bekki & Yong 2012; Marino et al. 2014). At first, van den Bergh (1996), and later Carretta et al. (2010), joined the two hypotheses into one and suggested that NGC 1851 may have been formed by the merger between parental globulars that were once located within a dwarf spheroidal galaxy.

A crucial piece of information about the NGC 1851 stellar subcomponents can be brought by way of a robust investigation of A(C+N+O) abundances. The importance of A(C+N+O) abundances was pointed out already by Milone et al. (2008) and by many other investigators (e.g. Cassisi et al. 2008; Villanova et al. 2010; Alves-Brito et al. 2012; Gratton et al. 2012a; Yong et al. 2015; Mészáros et al. 2021 and references therein). With knowledge of the A(C+N+O) abundance, it is possible to answer the question whether a spread in the subgiant branch is caused by the difference in A(C+N+O) or in age, as He has a small effect and the required difference in [Fe/H] would show up elsewhere in the colour-magnitude diagram (cf. Gratton et al. 2012b).

In this study, we investigate abundances of CNO and 26 other chemical elements for a sample of 45 RGB stars of NGC 1851 in a framework of the *Gaia*-ESO Public Spectroscopic Survey (Gilmore et al. 2012; Randich et al. 2013). The detailed elemental content of NGC 1851 stars is a crucial observational constraint to test the proposed globular cluster formation scenarios.

The structure of the paper is as follows. In Sect. 2, we present the observational data and analysis methods. In Sect. 3 we discuss the results of the abundance analysis. Our conclusions are drawn in Sect. 4.

2. Observations and method of analysis

NGC 1851 is an accessible observational target: relatively close ($D = 12.1$ kpc) and massive ($M = 3.2 \times 10^5\,M_\odot$, Baumgardt & Hilker 2018), with low reddening ($E(B-V) = 0.02$, Harris 1996, 2010 edition). Its halo-like orbit (Dinescu et al. 1999) results in a radial velocity of 320.5 km s^{-1}, making its stars clearly distinguishable from Galactic field stars in the same line of sight. The target selection strategy is described by Pancino et al. (2017b).

Observations were conducted with the multi-object instrument Fibre Large Array Multi-Element Spectrograph (FLAMES, Pasquini et al. 2002) on the Very Large Telescope (VLT) of the European Southern Observatory (ESO). The fibre link to UVES (Ultraviolet and Visual Échelle Spectrograph, Dekker et al. 2000) was used to obtain high-resolution spectra (R = 47 000) in a wavelength interval of 4700−6840 Å with a gap of about 50 Å in the centre. For the analysis we used both newly observed and ESO archival spectra from the previous programmes (083.D-0208, 084.D-0470, 084.D-0693, 088.B-0403, 092.D-0171). The spectra of the analysed NGC 1851 stars are stored in the *Gaia*-ESO survey operational database[1].

The spectra were reduced with the ESO UVES pipeline and dedicated scripts described by Sacco et al. (2014). Additional efforts were applied in improving their continuum

[1] The operational database has been developed by the Cambridge Astronomical Survey Unit (CASU) based at the Institute of Astronomy at the University of Cambridge. See the website http://casu.ast.cam.ac.uk/gaiaeso/ for more information.

Table 1. Main data on the NGC 1851 cluster target stars.

GES ID	ID (*)	RA (J2000)	Dec (J2000)	V (mag)	B (mag)	RV (km s^{-1})	S/N blue (**)	S/N red (**)	$v \sin i$ (km s^{-1})
Metal-poor									
05133868–4007395	14080	78.4112	−40.1276	14.320	15.560	319.92 ± 0.57	58	78	4.3 ± 0.6
05134936–4003160		78.4557	−40.0544	13.473	15.021	321.47 ± 0.57	99	161	6.5 ± 0.9
05135303–4000431	43466	78.4710	−40.0120	14.080	15.323	320.65 ± 0.57	122	213	4.2 ± 0.3
05135346–3958452	46958	78.4728	−39.9792	16.193	17.054	316.73 ± 0.12	31	43	3.8 ± 0.5
05135765–4004312	25037	78.4902	−40.0753	16.091	16.959	323.39 ± 0.11	44	63	3.8 ± 0.5
05135868–4000122		78.4945	−40.0034	14.945	15.963	325.03 ± 0.57	75	105	3.9 ± 0.5
05135918–4002496		78.4966	−40.0471	14.959	15.832	311.14 ± 0.57	95	155	6.5 ± 0.8
05135946–4005226		78.4978	−40.0896	14.734	15.813	315.63 ± 0.57	44	63	3.6 ± 0.7
05135977–4002009	37759	78.4990	−40.0336	14.615	15.666	313.47 ± 0.57	65	82	4.2 ± 0.3
05140044–4004135	26271	78.5018	−40.0704	13.456	14.957	326.37 ± 0.57	126	241	6.2 ± 0.5
05140069–4003242		78.5029	−40.0567	14.568	15.609	321.23 ± 0.57	57	90	4.0 ± 0.5
05140180–4002525		78.5075	−40.0479	14.684	15.727	311.70 ± 0.57	43	61	4.0 ± 0.2
05140260–4000223		78.5108	−40.0062	15.644	16.564	320.47 ± 0.11	50	72	4.0 ± 0.3
05140778–4001183	41198	78.5324	−40.0218	14.807	15.843	317.20 ± 0.57	51	79	3.7 ± 0.5
05140850–4005545	21453	78.5354	−40.0985	15.837	16.740	316.59 ± 0.11	43	59	4.3 ± 0.3
05141054–4003192		78.5439	−40.0553	14.261	15.399	315.90 ± 0.57	59	80	4.5 ± 0.3
05141057–4003308		78.5440	−40.0586	14.947	15.843	320.22 ± 0.57	93	147	5.9 ± 0.5
05141074–4004189	25859	78.5448	−40.0719	14.263	15.425	329.22 ± 0.57	76	95	4.1 ± 0.2
05141171–3959545	45413	78.5488	−39.9985	16.151	17.009	313.40 ± 0.11	36	52	4.0 ± 0.3
05141415–3957357	47698	78.5590	−39.9599	15.823	16.691	319.49 ± 0.57	40	57	4.4 ± 0.3
05141453–4002135	36584	78.5605	−40.0371	14.479	15.590	320.90 ± 0.57	54	76	4.1 ± 0.3
05141576–4003299		78.5657	−40.0583	14.167	15.346	320.05 ± 0.57	115	194	4.0 ± 0.2
05141957–4004055		78.5815	−40.0682	14.427	15.539	327.83 ± 0.57	72	96	4.5 ± 0.8
05141979–4006446	20426	78.5825	−40.1124	16.441	17.285	319.97 ± 0.12	30	45	3.8 ± 0.5
05141988–4003234	30286	78.5828	−40.0565	13.855	15.150	318.66 ± 0.57	96	169	4.9 ± 0.5
05142070–4004195		78.5863	−40.0721	16.503	17.324	320.74 ± 0.12	28	43	3.8 ± 0.3
05142530–4001361	39801	78.6054	−40.0267	13.649	15.038	327.17 ± 0.57	93	130	5.8 ± 0.5
05142875–4003159		78.6198	−40.0544	14.892	15.889	325.28 ± 0.57	44	62	4.1 ± 0.3
Metal-rich									
05134382–4001154	16120	78.4326	−40.0209	15.999	16.879	317.70 ± 0.11	50	65	3.9 ± 0.8
05134740–4004098	26552	78.4475	−40.0694	16.073	16.999	320.96 ± 0.11	34	50	3.9 ± 0.3
05135030–4002071	37220	78.4596	−40.0353	14.875	15.971	321.44 ± 0.57	41	60	4.0 ± 0.6
05135599–4004536	23765	78.4833	−40.0816	15.837	16.771	319.50 ± 0.10	36	53	3.6 ± 0.6
05135634–4003448	28520	78.4848	−40.0624	14.047	15.305	326.18 ± 0.57	73	117	4.6 ± 0.6
05135884–4003365	29203	78.4951	−40.0601	15.130	16.159	317.01 ± 0.10	80	137	4.2 ± 0.3
05135900–3959591	45257	78.4958	−39.9998	16.431	17.312	321.94 ± 0.57	31	45	4.0 ± 0.6
05140376–4001458		78.5157	−40.0294	15.064	16.069	315.93 ± 0.57	80	137	4.4 ± 0.3
05141447–4001109	41689	78.5603	−40.0197	14.335	15.531	321.87 ± 0.57	64	93	4.1 ± 0.2
05141566–4000059	45006	78.5653	−40.0016	16.234	17.120	314.78 ± 0.11	33	50	3.9 ± 0.3
05141615–4001502		78.5673	−40.0306	16.015	16.994	314.11 ± 0.57	49	71	3.9 ± 0.3
05141638–4003542	27715	78.5683	−40.0651	15.687	16.618	317.81 ± 0.57	47	66	3.9 ± 0.3
05141713–4004039	26928	78.5714	−40.0678	16.224	17.066	314.91 ± 0.57	32	51	4.0 ± 0.6
05142480–4002227	35750	78.6033	−40.0396	15.896	16.811	317.76 ± 0.11	38	64	3.8 ± 0.3
05142530–4000583		78.6054	−40.0162	16.329	17.159	319.76 ± 0.57	22	36	5.8 ± 0.5
05142597–4002538	32903	78.6082	−40.0483	13.842	15.224	321.50 ± 0.57	85	126	5.2 ± 0.6
05142892–4004454		78.6205	−40.0793	14.548	15.671	325.23 ± 0.57	53	77	4.2 ± 0.3

Notes. (*)Star IDs are from Carretta et al. (2011), V and B magnitudes from Stetson et al. (2019). The stars were divided into the metal-poor and metal-rich sub-samples according to criteria described in Sect. 3.1. (**)The median S/N values per pixel in the blue wavelengths at λ 4800−5750 Å, and in the red wavelengths at λ 5850−6800 Å, accordingly.

normalisation. For this purpose, we used the SPLAT-VO code[2]. Radial velocities (RV) and rotation velocities ($v \sin i$) were also determined by cross-correlating all the spectra with a sample of synthetic templates specifically derived for the *Gaia*-ESO project. The typical uncertainty on RVs is about 0.4 km s^{-1}. A list of the investigated 45 stars in NGC 1851 is presented in Table 1. The stars in Table 1 are divided into the metal-poor and metal-rich sub-samples according to criteria described later in Sect. 3.1. Figure 1 shows positions of the investigated stars on a colour magnitude diagram and Fig. 2 their positions around the cluster centre. Information on stellar positions and photometry

[2] http://star-www.dur.ac.uk/~pdraper/splat/splat-vo/splat-vo.html

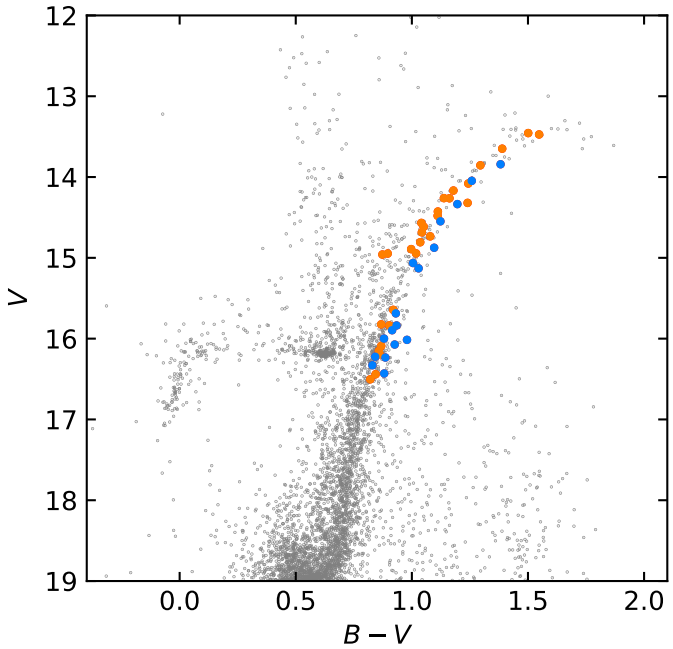

Fig. 1. V, $B-V$ colour-magnitude diagram of NGC 1851 (grey circles). Superimposed as larger blue and orange filled circles are the giants investigated in this study. The blue symbols are for the metal-rich subsample stars and the orange symbols are for the metal-poor stars (see the text for the description of how the stars were separated into these subsamples). The photometric data were taken from Stetson et al. (2019); namely, the earlier database version corresponding to the one presented in Monelli et al. (2013).

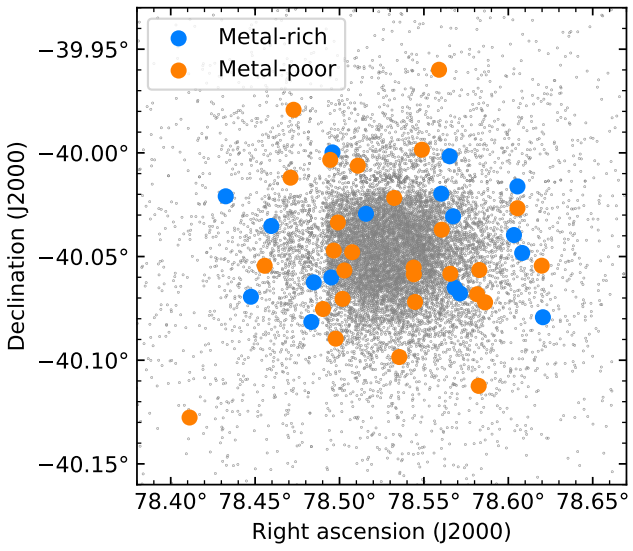

Fig. 2. Locations of the investigated NGC 1851 stars (Stetson et al. 2019). The investigated stars are marked by the blue symbols (the metal-rich subsample) and by the orange symbols (the metal-poor stars).

was taken from a catalogue by Stetson et al. (2019)[3], the earlier database version corresponding to the one presented in Monelli et al. (2013).

In this study, we use the main stellar atmospheric parameters and abundances of chemical elements presented in the fourth *Gaia*-ESO survey internal data release. They were determined spectroscopically using a differential model atmosphere technique described by Smiljanic et al. (2014). In short, as the *Gaia*-ESO covers a wide range of targets, the spectra from high-resolution UVES observations were analysed in parallel by several nodes of scientists of the *Gaia*-ESO Consortium. Each of them adopted a slightly different approach or software (or both) with the aim to best cover the whole parameter space. On the other hand, all the nodes used a common line list (Ruffoni et al. 2014; Heiter et al. 2021, and references therein), a set of MARCS[4] model atmospheres by Gustafsson et al. (2008), solar abundances by Grevesse et al. (2007), and analysed common calibration targets (Pancino et al. 2017b).

It was a two-stage approach. First, every node determined the atmospheric parameters. Then, using the *Gaia* benchmark stars (Jofré et al. 2014; Heiter et al. 2015), the systematic and random errors affecting each node and correlations among the nodes were inferred by means of a Bayesian MCMC model. This model was then applied to the survey data to estimate the best values of the atmospheric parameters and their uncertainties. After this process, a single set of recommended parameters was provided, and the nodes proceeded to the second step of determining the elemental abundances. In this case, the nodes were asked to provide abundance values for the individual spectral lines of each chemical species that were analysed. The method to homogenise the abundances was similar to the one used for the atmospheric parameters, but there were no reference abundances to rely on. In this case, the repeated measurements in different spectra of the same stars and the measurements of multiple spectral lines (when possible) helped to constrain the correlations and typical uncertainties of each node. A full description of the homogenisation, applied to the last *Gaia*-ESO data releases, will be described by Worley et al. (in prep.). Approximate uncertainties of the main atmospheric parameters in the case of NGC 1851 are ±100 K, ±0.25 dex, and ±0.1 dex for $T_{\rm eff}$, $\log g$, and [Fe/H], respectively.

Abundances of carbon and nitrogen were determined using the same method as in Tautvaišienė et al. (2015). The C_2 Swan (1,0) band head at 5135.6 Å and C_2 Swan (0,1) band head at 5635.2 Å were investigated in order to determine the carbon abundance. The C_2 bands are suitable for carbon abundance investigations since they give the same carbon abundances as [C I] lines, but are not sensitive to non-local thermodynamic equilibrium (NLTE) deviations (cf. Clegg et al. 1981; Gustafsson et al. 1999). Since abundances of C and O are bound together by the molecular equilibrium in the stellar atmosphere the oxygen abundance was determined as well. For this purpose, we used the forbidden [O I] line at 6300.3 Å. Following Johansson et al. (2003), we took into account the oscillator strength values for ^{58}Ni and ^{60}Ni, which blend the oxygen line. Lines of [O I] are considered as very good indicators of oxygen abundances. It was determined that they are not only insensitive to NLTE effects, but also give quite similar oxygen abundance results with 3D and 1D model atmospheres (cf. Asplund 2004; Pereira et al. 2009). This line forms in near-LTE and is only weakly sensitive to convection, its formation is similar in 3D radiation hydrodynamic and 3D magneto radition-hydrodynamical solar models (Bergemann et al. 2021). For the analysis only, we used lines unaffected by the telluric contamination. The interval 6470−6490 Å containing ^{12}C^{14}N bands was used for the nitrogen abundance analysis. All the synthetic spectra have been calibrated to the solar spectrum by Kurucz (2005) to make the

[3] https://www.canfar.net/storage/list/STETSON

[4] http://marcs.astro.uu.se/

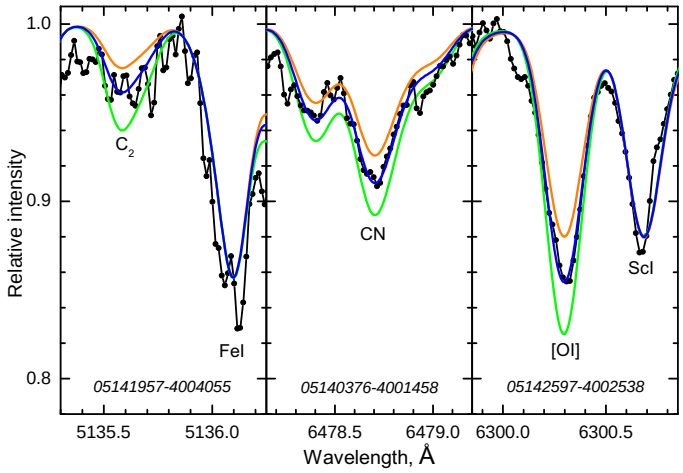

Fig. 3. Fits to the C_2, CN, and forbidden [O I] line in the spectra of three NGC 1851 stars. The observed spectra are shown as black lines with dots. The best-fit synthetic spectra are the blue lines with ±0.1 dex changes in corresponding abundances shown as orange and green lines.

Table 2. Effects of derived abundances and isotopic ratios for the star NGC 1851 05141576–4003299, resulting from abundance changes of C, N, or O.

Species	ΔC ±0.1 dex	ΔN ±0.1 dex	ΔO ±0.1 dex
ΔC	–	±0.01	±0.04
ΔN	∓0.11	–	±0.08
ΔO	±0.01	0.00	–
ΔC/N	±0.15	∓0.15	0.00

analysis strictly differential. We used a spectrum synthesis code *Turbospectrum* (Plez 2012).

In fitting the observed and the theoretical spectra, the stellar rotation (provided in Table 1) was taken into account. Approximate values of stellar rotation velocities were evaluated for the Survey stars as described by Sacco et al. (2014) and provided in the *Gaia*-ESO Survey GES iDR4 database. The values of $v \sin i$ were calculated using an empirical relation of a full width half maximum of the cross-correlation function (CCF_{FWHM}) and $v \sin i$, which was specifically derived for this project. Figure 3 displays examples of spectrum syntheses for the programme stars.

We applied the NLTE corrections to abundances of Li, Na, and Ba, as they have the most sensitive lines. The Li NLTE corrections were computed for every star using the code provided by Wang et al. (2021). The averaged value of all these corrections is -0.07 ± 0.02 dex. For the sodium abundances, the corrections were taken from Lind et al. (2011) and their averaged value is -0.08 ± 0.03 dex. For the barium abundances, the NLTE corrections were taken from Korotin et al. (2014) and their averaged value is -0.09 ± 0.04 dex.

We estimated uncertainties on abundances by taking into account the uncertainties in the atomic data, continuum placement variations, and imperfect equivalent width measurements or the fitting of synthetic spectra to each line, as well as uncertainties in the stellar atmospheric parameters. The abundance uncertainties of all the investigated chemical elements for every star are provided along with the abundance results.

As C, N, and O are linked through molecular equilibrium in the atmospheres of the cool giants we are studying, we must also consider how an uncertainty in one element's abundance would affect the other two. This is summarised in Table 2 for the star NGC 1851 05141576–4003299, which is near the median of $T_{\rm eff}$ and $\log g$ in our sample. We refer to Smiljanic et al. (2014) and Tautvaišienė et al. (2015) for more details about the method of analysis and uncertainties.

3. Results and discussion

The main atmospheric parameters and elemental abundances in stars of the globular cluster NGC 1851 are presented in Table 3, a full version of which is provided in an electronic form. The $\log g$, $T_{\rm eff}$ diagram of the investigated stars is presented in Fig. 4 and the determined abundances in Figs. 5–7.

3.1. Two stellar populations in NGC 1851

It has been suspected that NGC 1851 is not chemically homogeneous since the spectroscopic study of Hesser et al. (1982), which found "extraordinarily strong" CN bands in three of eight red giant stars, indicating large star-to-star variations probably in nitrogen abundance. Those authors also identified variations in the abundance of Ba and Sr, namely, elements produced by the *s*-process. There have been a number of studies of the complexity in the chemical compositions of stars in NGC 1851, revealing two populations of stars, very distinct in their nitrogen and *s*-process dominated element abundances.

We separated NGC 1851 stars between metal-rich and metal-poor ones according to their abundances of iron, nitrogen, and *s*-process dominated elements. Figure 8 shows that the stars fall into two clear subsamples according to their mean abundances of *s*-process dominated elements and nitrogen-to-iron ratios. As the nitrogen abundances in GES iDR4 were determined for only part of the sample of stars (since the lines of C_2 were too week for the robust carbon abundance determination and, consequently, we were not able to determine the nitrogen abundance from CN lines), we decided to check the strength of CN lines and try to overcome this problem for stars with clearly visible CN lines. We found that nine stars had the CN lines clearly visible. We accepted the mean value of carbon abundance calculated for the subsample of nitrogen rich stars and determined approximate values of their nitrogen abundances. As the scatter of the mean carbon abundance is quite small, those values of nitrogen determination should be rather accurate. We plotted them as empty circles in Fig. 8. The stars that had the CN lines almost invisible were attributed to the metal-poor subsample with low nitrogen abundance. The division of the whole sample is shown in Fig. 9. The hardest separation between the two subsamples is at the mean value of *s*-process dominated elements of 0.1 dex. Only one star is slightly above this value, however, its nitrogen and iron abundances are low; thus we attributed it to the metal-poor subsample. The stellar density distributions are also presented and we can see the two clear populations of stars. In [N/Fe] and [Fe/H], there is some overlap in abundance distribution tails due to a natural spread and uncertainties. In Table 4, we present the averaged elemental abundances and their ratios for the two populations of investigated NGC 1851 stars. Abundance ratios to iron of α-elements, iron-peak elements, and the *r*-process-dominated element europium in both subsamples are very similar. However, differences in other chemical elements are noticeable.

Table 3. Main atmospheric parameters and elemental abundances in stars of the globular cluster NGC 1851.

Star	$T_{\rm eff}$	$e\_T_{\rm eff}$	$\log g$	$e\_\log g$	[Fe/H]	e_[Fe/H]	$v_{\rm t}$	$e\_v_{\rm t}$	Al I			...	C/N
	(K)	(K)					(km s^{-1})	(km s^{-1})	[El/H]	σ	nl		
05141988−4003234	4215	153	0.86	0.39	−1.16	0.12	1.74	0.09	−1.03	0.07	3	...	
05135918−4002496	4856	111	1.50	0.23	−1.13	0.09	1.82	0.11	−0.74	0.07	3	...	0.72
05141057−4003308	4808	114	1.51	0.23	−1.12	0.10	1.69	0.04	−0.89	0.07	3	...	0.58
05134936−4003160	3988	318	0.51	0.77	−1.11	0.18	2.16	0.05	−0.69	0.07	3	...	0.78
05141074−4004189	4407	124	1.18	0.25	−1.09	0.10	1.59	0.03	−0.98	0.07	3	...	
05141576−4003299	4374	118	1.18	0.22	−1.08	0.10	1.56	0.05	−0.84	0.07	3	...	0.65
05133868−4007395	4419	124	1.25	0.25	−1.08	0.10	1.66	0.04	−0.91	0.07	3	...	0.91
05140850−4005545	4843	135	1.98	0.29	−1.07	0.11	1.45	0.03	−0.47	0.07	3	...	
05135303−4000431	4378	126	1.14	0.25	−1.07	0.11	1.63	0.04	−0.95	0.07	3	...	0.81
05141171−3959545	4823	120	2.14	0.23	−1.07	0.10	1.43	0.03	−0.53	0.07	3	...	

Notes. We show here a part of Table 3 to display the structure and content. The whole table can be found in electronic form at the CDS. It contains the main atmospheric parameters and determined abundances for up to 28 chemical elements in 45 starts of NGC 1851. "Star" – the GES target identifier, "$T_{\rm eff}$" – effective temperatures, "$e\_T_{\rm eff}$" – uncertainty of the effective temperature, "$\log g$" – surface gravity, "$e\_\log g$" – uncertainty of surface gravity, "[Fe/H]" – metallicity, "e_[Fe/H]" – uncertainty of metallicity, "$v_{\rm t}$" – microturbulent velocity, "$e\_v_{\rm t}$" – uncertainty of microturbulent velocity, "[El/H]" – element abundance in relation to hydrogen, "σ" – abundance scatter between multiple lines for the same star, "nl" – number of lines used for the abundance determination.

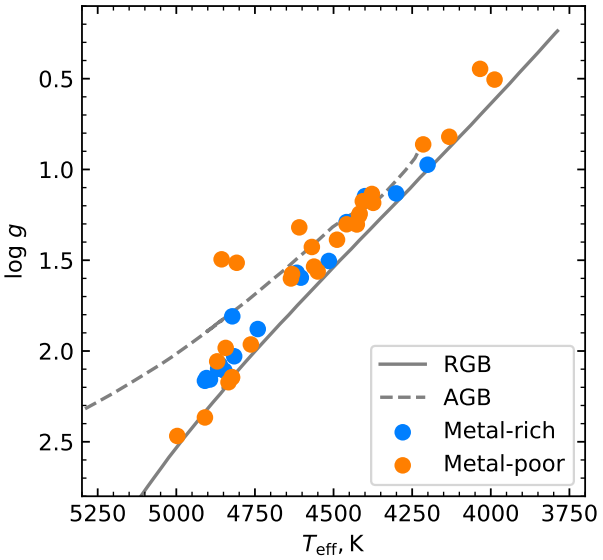

Fig. 4. Log g, $T_{\rm eff}$ diagram of the investigated NGC 1851 stars together with the PARSEC (Bressan et al. 2012) isochrone of the mean Age = 12.27 Gyr (Valcin et al. 2020) and [Fe/H] = −1.0.

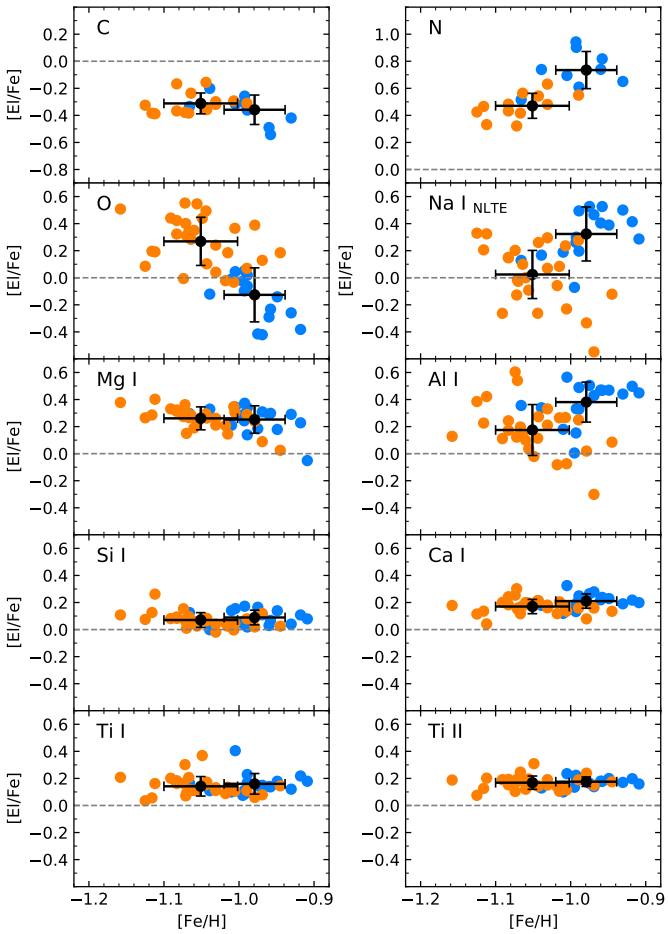

Fig. 5. Stellar relative abundances [El/Fe] of light elements in respect to [Fe/H] for metal-rich (blue symbols) and metal-poor stars (orange symbols) stars. The average values of the metal-rich and metal-poor samples of stars are shown in black.

3.2. Metallicity

Thus, the investigated stars were divided into the subsamples of 17 metal-rich and 28 metal-poor stars with averaged metallicities of −0.98 ± 0.04 dex and −1.05 ± 0.05 dex, respectively. We performed a significance test for those subsamples and we obtained a p-value as low as 1×10^{-5}, which demonstrates the probability that this [Fe/H] difference could have occurred just by chance. Carretta et al. (2010, 2011) have demonstrated that the s-rich and s-poor subsamples of stars in NGC 1851 also differ in metallicity by about 0.07−0.08 dex. Those authors suggested that NGC 1851 might be the result of a merger of two globular clusters, as proposed by van den Bergh (1996), and their age difference could be 1 Gyr. A metallicity difference of about 0.07 dex was also determined by Gratton et al. (2012a), who analysed giants and horizontal-branch stars. The mean [Fe/H] values in the metal-rich and metal-poor populations investigated in our work also differ by 0.07 dex, although the absolute metallicity values are slightly different in various studies due to differences in the methods of analysis. It has been investigated whether the NLTE effects on Fe I lines could cause the metallicity spread or bimodal iron abundances in some globular clusters (e.g. Mucciarelli et al. 2015; Lee 2016; Kovalev et al. 2019). As we see in Fig. 3 by Kovalev et al. (2019), the NLTE effects in the

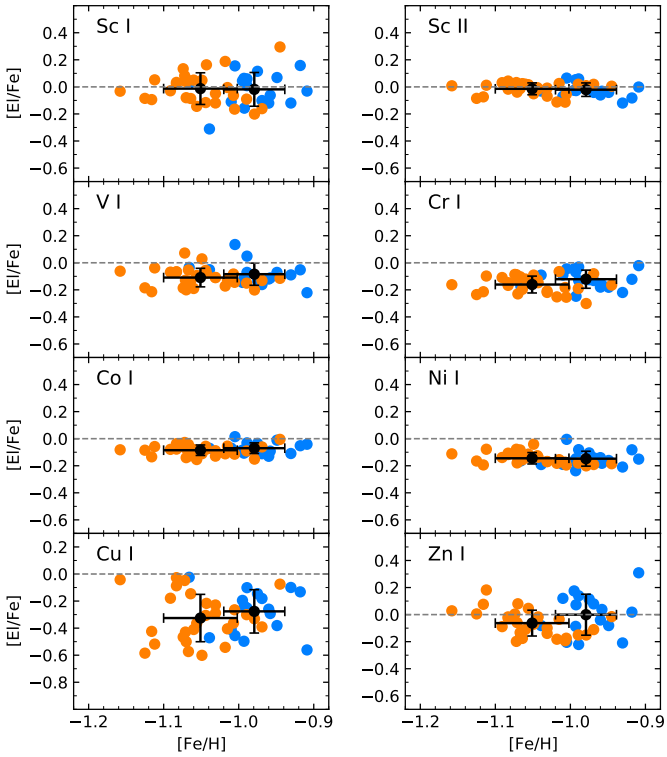

Fig. 6. Stellar relative abundances [El/Fe] of iron group elements in respect to [Fe/H].

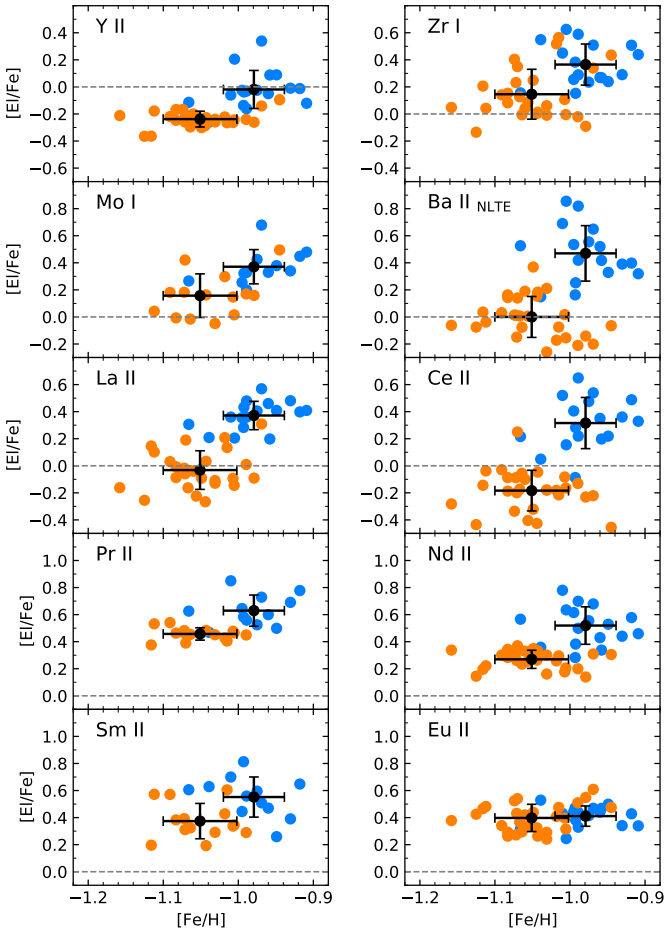

Fig. 7. Stellar relative abundances [El/Fe] of neutron-capture elements in respect to [Fe/H]. The meanings of the symbols are the same as in Fig. 5.

NGC 1851 parameters are very small. They can be larger in more metal-deficient globular clusters when stronger spectral lines are used for the analysis.

3.3. Elements produced by s-process

In our study, the mean values for two subsamples of stars in averaged *s*-process element abundances are 0.01 ± 0.08 dex and 0.34 ± 0.11 dex for the metal-poor and metal-rich subsamples, respectively. Yong & Grundahl (2008) confirmed the *s*-process variations noted by Hesser et al. (1982) and suggested that the s-rich and s-poor abundance groups might correspond to the two photometrically identified subgiant branches. Gratton et al. (2012a) investigated elemental abundances of stars in the two subgiant branches of NGC 1851 and found that the fainter one is composed by metal-rich and *s*-process-element-rich stars, and the brighter on has metal-poor and *s*-process-element-poor stars. In our study, as well as that of Carretta et al. (2011), we see the same relation between metallicity and *s*-process dominated element abundances.

3.4. Light elements

The metal-rich and metal-poor subsamples have very similar carbon abundances but distinct abundances of nitrogen and consequently different values of C/N ratios. Figure 10 shows where the sampled stars are located in the C/N versus log *g* and [Fe/H] planes. The mean value of the C/N ratio in the metal-rich stars is 0.35 ± 0.13, and 0.66 ± 0.13 in metal-poor stars. In NGC 1851, Lim et al. (2015) also found no difference in strengths of CH lines between the two groups of stars with different CN strengths, while they found that CN and CH are anticorrelated in NGC 288 and a positive correlation is in M 22. In another *Gaia*-ESO survey paper, Lagarde et al. (2019) showed that C and N abundances in NGC 1851 are reproduced well with the thermohaline mixing only (their Fig. 8).

Differences among the two populations are also present in the abundances of oxygen and sodium (Fig. 5), and both populations exhibit Na-O anticorrelations (Fig. 11). In stellar samples investigated by Carretta et al. (2010, 2011), the Na-O anticorrelation was present to the same degree in both the relatively metal-rich and relatively metal-poor stars. Gratton et al. (2012c) also found a Na-O anti-correlation among blue horizontal branch stars, which partially overlaps that which is found among red horizontal branch stars, although the blue horizontal branch stars were found to be more Na-rich and O-poor overall.

The lithium abundances are not significantly larger in the metal-rich population of stars (see Figs. 12 and 13, where the upper values of abundances are shown by empty symbols). The difference in the averaged Li abundance values (Table 4) may be caused by a selection factor. Also, there is no correlation between the Li abundances and [Na/Fe] abundance ratios (Fig. 14). The *Gaia*-ESO Survey dataset of about a dozen globular clusters observed will enable the expansion of the statistical investigation of the Li behaviour in globular clusters. In addition, it will foster further theoretical studies of stellar evolution and provide new insights into the multiple stellar population problem in globular clusters (see the recent overview by Sanna et al. 2020). As yet, a complete understanding of the light-element patterns and

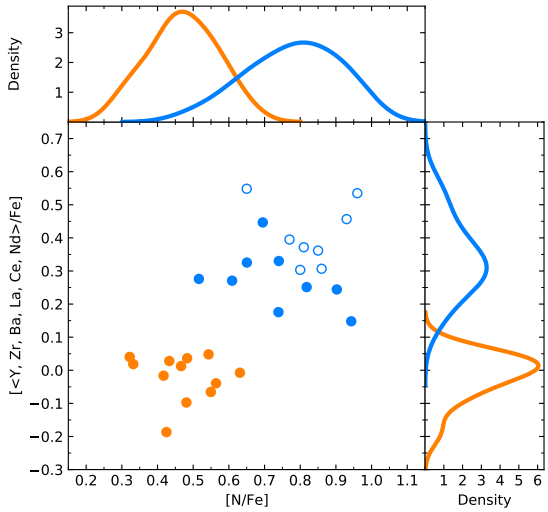

Fig. 8. Averaged abundances of the *s*-process dominated chemical elements in respect to [N/Fe] for stars in metal-rich (blue symbols) and metal-poor (orange symbols) populations. The text provides an explanation of the empty blue symbols.

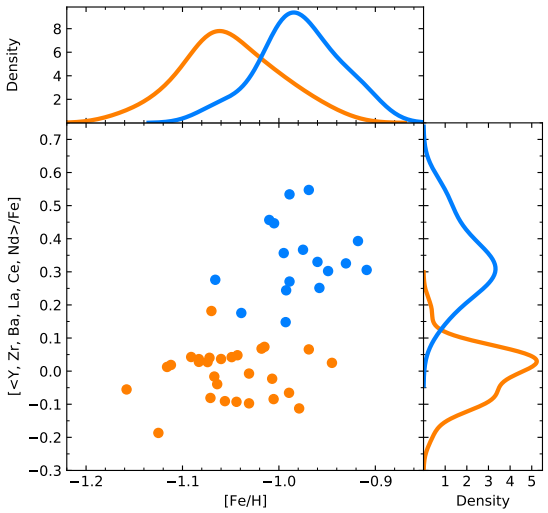

Fig. 9. Averaged abundances of the *s*-process dominated chemical elements in respect to [Fe/H]. The meanings of the symbols are the same as in Fig. 8.

evolution has not been achieved (see Randich & Magrini 2021 for a review).

4. Formation scenario for NGC 1851

4.1. A hint of different ages and the two-cluster merger based on C, N, and O abundances

There have been a number of studies that found that strengths of CN bands vary in stars of NGC 1851 quite significantly (e.g. Pancino et al. 2010; Lardo et al. 2012). Moreover, Campbell et al. (2012) and Simpson et al. (2017) updated the picture by finding in low-resolution spectra of red giants and asymptotic giant branch stars a quadrimodal distribution of CN band strengths, which could be explained by a superposition of two bimodal populations of two merged clusters. Our results also show spreads of the C/N ratios in both subsamples. As in our study, low-resolution spectral investigations of larger samples

Table 4. Averaged abundances for the two populations and numbers of stars.

Parameter	Metal-poor			Metal-rich		
	Average	σ	N	Average	σ	N
[Fe/H]	−1.05	0.05	28	−0.98	0.04	17
A(Li I) $_{\rm 3D\,NLTE}$	0.14	0.66	27	0.46	0.59	17
[C/Fe] (C_2)	−0.31	0.08	14	−0.36	0.11	9
[N/Fe] (CN)	0.47	0.09	12	0.73	0.14	9
[O/Fe] ([O I])	0.27	0.18	28	−0.13	0.20	16
[Na I/Fe] $_{\rm NLTE}$	0.02	0.23	25	0.32	0.17	16
[Mg I/Fe]	0.26	0.08	28	0.25	0.10	17
[Al I/Fe]	0.17	0.19	28	0.38	0.15	17
[Si I/Fe]	0.07	0.05	28	0.09	0.05	17
[Ca I/Fe]	0.17	0.05	28	0.21	0.05	17
[Ca II/Fe]	0.24	0.12	25	0.29	0.15	15
[Ti I/Fe]	0.14	0.07	28	0.16	0.08	17
[Ti II/Fe]	0.17	0.05	28	0.18	0.04	17
[Sc I/Fe]	−0.01	0.12	28	−0.02	0.12	17
[Sc II/Fe]	−0.01	0.04	28	−0.02	0.05	17
[V I/Fe]	−0.11	0.07	28	−0.08	0.08	17
[Cr I/Fe]	−0.16	0.06	28	−0.12	0.07	17
[Cr II/Fe]	0.04	0.11	27	−0.05	0.08	17
[Mn I/Fe]	−0.37	0.05	28	−0.41	0.05	17
[Co I/Fe]	−0.09	0.04	28	−0.07	0.04	17
[Ni I/Fe]	−0.14	0.04	28	−0.15	0.06	17
[Cu I/Fe]	−0.33	0.17	28	−0.28	0.16	17
[Zn I/Fe]	−0.06	0.10	28	0.00	0.15	17
[Y II/Fe]	−0.24	0.06	28	−0.02	0.14	17
[Zr I/Fe]	0.15	0.18	27	0.37	0.15	17
[Mo I/Fe]	0.16	0.16	14	0.37	0.13	12
[Ba II/Fe]	0.10	0.13	28	0.55	0.19	17
[Ba II/Fe] $_{\rm NLTE}$	0.00	0.15	28	0.47	0.20	17
[La II/Fe]	−0.03	0.14	27	0.37	0.10	17
[Ce II/Fe]	−0.18	0.15	28	0.32	0.19	17
[Pr II/Fe]	0.46	0.05	15	0.63	0.12	12
[Nd II/Fe]	0.27	0.07	28	0.52	0.14	17
[Sm II/Fe]	0.37	0.13	14	0.55	0.15	12
[Eu II/Fe]	0.40	0.10	28	0.41	0.07	17
A(C+N+O)	7.97	0.11	12	7.94	0.08	9
C/N	0.66	0.13	12	0.35	0.13	9
[α/Fe]	0.16	0.04	28	0.18	0.05	17
[Iron peak/Fe]	−0.09	0.04	28	−0.07	0.04	17
[s/Fe]	−0.01	0.08	28	0.34	0.11	17

of the cluster members exhibited the multi-modal behaviour in their CN, but not in their CH bands (Simpson et al. 2017; Lim et al. 2015). The high-precision photometric study of Milone et al. (2008) interpreted the two distinct subgiant branches in NGC 1851 as evidence for some combination of bimodalities in age and total [(C+N+O)/Fe] abundance. This latter possibility was supported by Yong et al. (2009, 2015), who in their study of 11 stars, found a difference of 0.6 dex in [(C+N+O)/Fe] between the two populations. A smaller spread in A(C+N+O) was obtained by Simpson et al. (2017) using medium-resolution spectra. Villanova et al. (2010) investigated high-resolution spectra of 15 RGB stars and, on the contrary, found that the two populations do not show any significant difference in their total A(C+N+O) content.

Our study shows that there is a spread of about ±0.1 dex in A(C+N+O) in both populations, however, the averaged values between the populations do not differ (see Fig. 15 and Table 4). Gratton et al. (2012a) evaluated that the metal-rich subsample would be older by ∼0.6 Gyr than the metal-poor if the total A(C+N+O) abundance is the same in both subsamples (see their Fig. 20). In addition, for instance, if the sum of A(C+N+O) were larger by a factor of 2 for metal-rich stars than for metal-poor stars, then the first would be found to be younger than the second by ∼0.4 Gyr; however, the actual values are almost fully inverted.

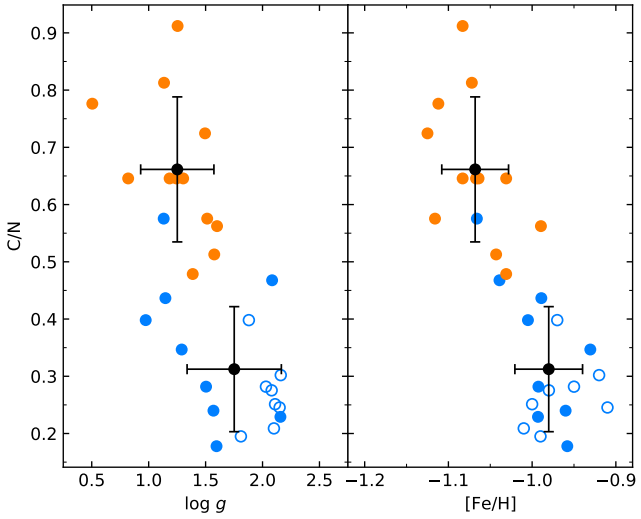

Fig. 10. C/N ratios in respect of the surface gravity and [Fe/H] values. The meanings of symbols are the same as in Fig. 8.

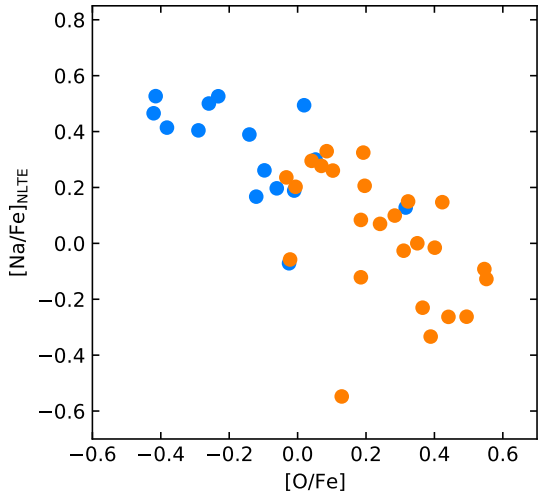

Fig. 11. [Na/Fe] in respect to [O/Fe]. The meanings of symbols are the same as in Fig. 8.

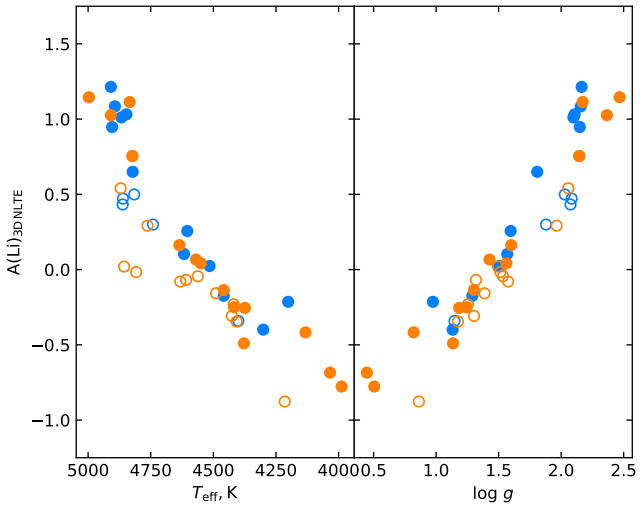

Fig. 12. Lithium abundances in respect of the effective temperature and surface gravity values for stars in metal-rich (blue symbols) and metal-poor (orange symbols) populations. The upper values of Li abundances are plotted by empty circles.

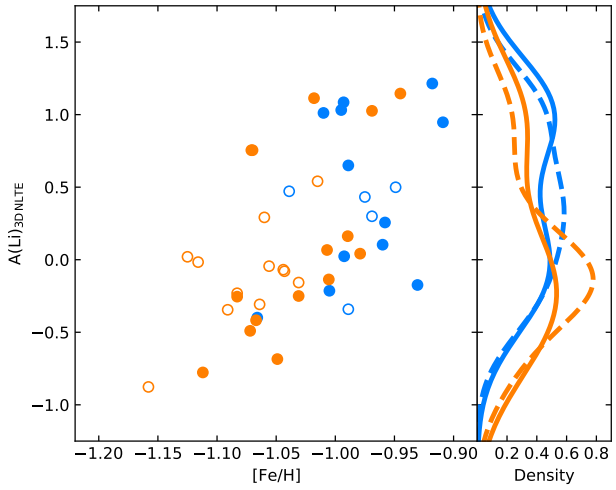

Fig. 13. Lithium abundances in respect of metallicity. The meanings of symbols are the same as in Fig. 12. The dashed lines indicate densities with the upper Li abundances included.

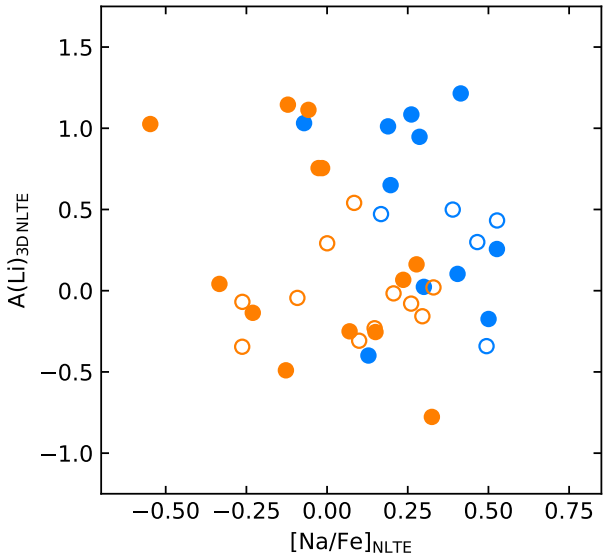

Fig. 14. Lithium abundances in respect of [Na/Fe]. The meanings of symbols are the same as in Fig. 12.

Thus, our robust analysis of C, N, and O abundances provides additional evidence that NGC 1851 is composed of two clusters, since the metal-rich cluster is by about 0.6 Gyr older than the metal-poor one. The recent overall age estimate for NGC 1851 is 12.27(+1.47/−0.98) Gyr (Valcin et al. 2020).

The older and metal-rich cluster has a different chemical composition pattern than the metal-poor one and might be formed from material enriched by ejecta of asymptotic giant branch stars or other polluters (e.g. de Mink et al. 2009; Bastian et al. 2013, 2015; Gieles et al. 2018).

While the possibility for globular clusters to merge in the Galactic halo seems unrealistic, this kind of merger can happen in dwarf galaxies. Numerical simulations by Bekki & Yong (2012) showed that two clusters can merge and form the nuclear star cluster of a dwarf galaxy. After the parent dwarf galaxy is accreted by the Milky Way, its dark matter halo and stellar envelope can be stripped by the Galactic tidal field, leaving behind the nucleus (i.e. NGC 1851) and a diffuse stellar halo.

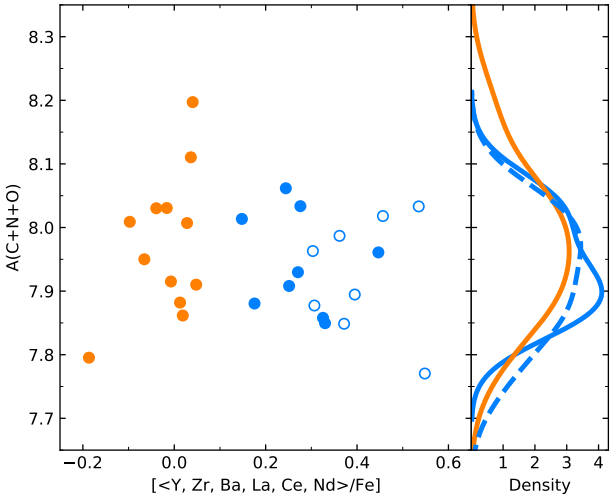

Fig. 15. A(C+N+O) abundances in respect to the averaged abundances of the *s*-process dominated chemical elements. The dashed blue line shows the density with the values marked by the empty symbols. The meaning of symbols is as in Fig. 8. The A(C+N+O) abundances are similar in both populations of NGC 1851 stars.

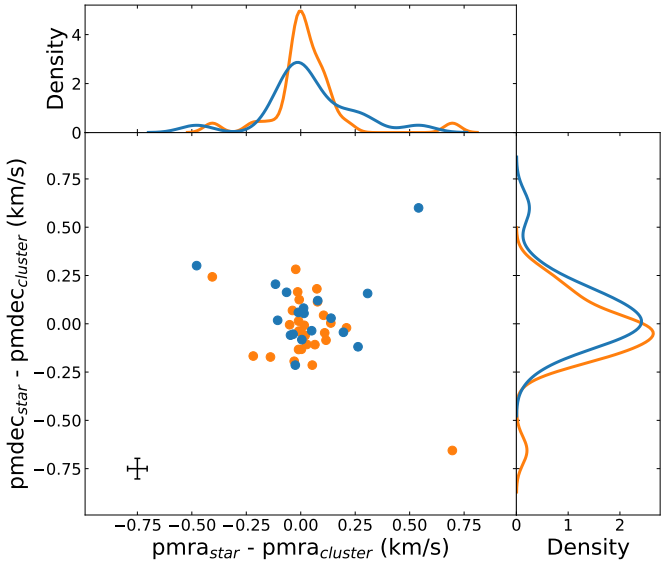

Fig. 16. Distribution of proper motions of stars in respect to the mean values of the cluster. The proper motions of the cluster stars were taken from the 2nd *Gaia* data release (Gaia Collaboration 2018). The meaning of symbols is as in Fig. 4.

In principle, stars from the two merged clusters could also have different kinematics, which would then be visible in their velocity distribution. We selected stellar proper motions measured by the *Gaia* space telescope (Gaia Collaboration 2016, 2018) and compared the metal-poor and metal-rich subsamples in Fig. 16. As in Carretta et al. (2011), we found no statistically significant differences. It would be good to have a comprehensive dynamical model, however, it is not known when the merging occurred and how the relaxation proceeded. If some debris from the parent galaxy of NGC 1851 still exists (as discussed in the next section), then the event could have taken place rather recently and the cluster is not yet relaxed.

4.2. Parent galaxy

A possibility that NGC 1851 originated at the nucleus of a dwarf galaxy that was captured by the Milky Way was supported by the work of Marino et al. (2014), who confirmed the presence of a diffuse 'halo' of stars co-moving with the cluster (noted by Olszewski et al. 2009) and found that it has the same chemical pattern as the *s*-process-poor stars within the cluster. Fifteen stars were interpreted as being part of the field population from the original dwarf galaxy. Navin et al. (2015) also found four probable extratidal cluster halo stars at distances up to ∼3.1 times the tidal radius (confirmed by Simpson et al. 2017), which support the notion that NGC 1851 is surrounded by an extended stellar halo. Kuzma et al. (2018) confirmed the existence of a large diffuse stellar envelope surrounding NGC 1851 of size at least 240 pc in radius. According to results of the RAVE survey reported by Kunder et al. (2014), stars that may be associated with NGC 1851 reach projected distances of about 10° away from the core of the cluster. These findings are rather reliable as the radial velocity and [Fe/H] abundance of NGC 1851 are largely offset from the Galactic disc field stars seen in projection along the line of sight; thus, the field star contamination issues can be easily resolved.

Marino et al. (2014) noted that NGC 1851 lies within the so-called 'Vast Polar Structure' of satellite galaxies of the Milky Way discussed in Pawlowski & Kroupa (2013) and references therein. The majority of satellite galaxies of the Milky Way define a thin plane perpendicular to the Galactic disc. Recently, based on the Early *Gaia* Data Release, Li et al. (2021) estimated proper motions of 46 dwarf galaxies of the Milky Way and found that between half and two-thirds of the satellites have orbital poles that indicate them to orbit along with the vast polar structure, with the vast majority of these co-orbiting in a common direction also shared by the Magellanic Clouds. This is indicative of the real structure of dwarf galaxies.

NGC 1851 was often compared with other globular clusters that have a spread of heavy chemical elements in their stars, such as M 22 or ω Centauri. Even though some similarities have been revealed, the formation and evolution histories of these star clusters were quite different. As an example, Lee (2020) found five populations in M 22 from Ca-CN-CH photometry. The metal-poor stars were divided into two subpopulations and the metal-rich stars into three subpopulations. They support the idea that M 22 was formed via a merger of two globular clusters. Mészáros et al. (2021) investigated multiple populations of ω Centauri by analysing APOGEE spectra and found seven populations based on stellar [Fe/H], [Al/Fe], and [Mg/Fe] abundances, as well as the increased A(C+N+O) with increased metallicity. The parent galaxies of these clusters also may be different.

Key data is derived from kinematics and ages. There is a number of recent studies based on the new *Gaia* space mission results that investigate what merger the peculiar NGC 1851 cluster and other clusters could be attributed to. For instance, Massari et al. (2019) attributed NGC 1851 to the *Gaia*-Enceladus (along with 25 other globular clusters and 6 tentative ones), while M 22 was attributed to the Galactic main disc, and ω Centauri was attributed to the *Gaia*-Enceladus or Sequoia merger event (Forbes 2020 is in favour of ω Centauri rather belonging to Sequoia).

According to Helmi et al. (2018), the *Gaia*-Enceladus was slightly more massive than the Small Magellanic Cloud. In Fig. 17, for the metal-rich and metal-poor NGC 1851 subsamples, we displayed the mean abundances of chemical elements

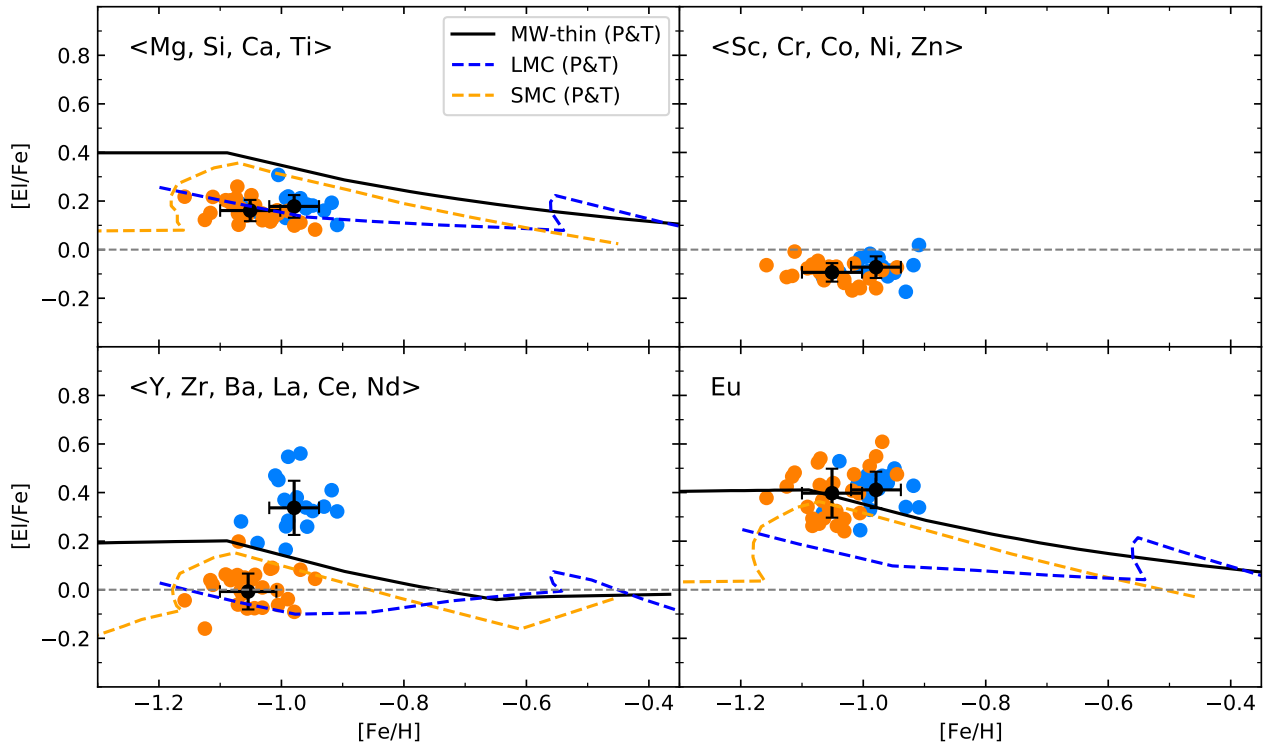

Fig. 17. Comparison of mean abundances of chemical elements dominated by different nucleosynthesis processes with the corresponding models of the Milky Way and the Large and Small Magellanic Cloud evolution by Pagel & Tautvaisiene (1995, 1997, 1998). The meaning of other symbols is as in Fig. 5.

dominated by different nucleosynthesis processes and compared with the corresponding semi-empirical models of the Large and Small Magellanic Clouds from Pagel & Tautvaisiene (1998) and to the Milky Way models from Pagel & Tautvaisiene (1995, 1997). It can be seen that NGC 1851 α-elemental abundances are lower than in the Milky Way and are very similar to those in the Large Magellanic Cloud, as well as to the model predictions at this metallicity compiled for the *Gaia*-Enceladus galaxy (see Fig. 2 Vincenzo et al. 2019). Abundances of the *r*-process dominated element europium are larger, meaning that in the progenitor *r*-process, elements were produced more efficiently relative to α-process elements. The abundance ratios of *s*-process dominated elements to iron in the metal-poor subsample are similar to the Large Magellanic Cloud. A similar pattern was found by (Matsuno et al. 2021) in a sample of 47 stars attributed to the *Gaia*-Enceladus in the GALAH survey (abundances of Mg, Fe, Ba, La, and Eu were determined). The authors also performed one-zone chemical evolution calculations and showed that high [Eu/Mg] and low [Mg/Fe] ratios can be explained by chemical enrichment from neutron star mergers and Type Ia supernovae. The elevated *r*-process element enrichment in four *Gaia*-Enceladus and five Sequoia stars was determined also by Aguado et al. (2021), as well as in two stars of the globular cluster NGC 1261 (associated with the *Gaia*-Enceladus) by Koch-Hansen et al. (2021). Thus, according to its chemistry, NGC 1851 fits the *Gaia*-Enceladus parent galaxy and even may be its nucleus as suggested by Bekki & Yong (2012) and Forbes (2020).

5. Summary and conclusions

In this work, we investigated abundances of 29 chemical elements in 45 giants of the globular cluster NGC 1851 using high-resolution spectra within the *Gaia*-ESO Public Spectroscopic Survey. The stars were separated to metal-rich and metal-poor subsamples according to their abundances of nitrogen and *s*-process dominated elements. Special attention was given to establishing a robust determination of C, N, and O abundances. Our results can be summarised as follows:

- The investigated stars can be separated into two subsamples with a difference of 0.07 dex in the mean metallicity. There are 17 metal-rich and 28 metal-poor stars, with averaged metallicities of -0.98 ± 0.04 dex and -1.05 ± 0.05 dex, respectively.
- The subsamples have a difference of 0.3 in the mean C/N and 0.35 dex in the mean [*s*/Fe] values.
- The two subsamples also differ in the mean abundances of oxygen, sodium, and aluminium, and both have Na-O anti-correlations.
- No significant difference was determined in the mean abundance to iron ratios of lithium, carbon, α- and iron-peak-elements, and of europium.
- There is a spread of about ± 0.1 dex in A(C+N+O) in both subsamples, however, the averaged values between the subsamples do not differ, which provides additional evidence that NGC 1851 is composed of two clusters, with the metal-rich cluster being by about 0.6 Gyr older than the metal-poor one.
- A global overview of NGC 1851 properties and the detailed abundances of chemical elements favour a formation scenario in a dwarf spheroidal galaxy accreted by the Milky Way.

In order to understand the complex history of the origins of globular clusters in the Milky Way, many more comprehensive studies will have to be accomplished.

Acknowledgements. Based on the *Gaia*-ESO Public Spectroscopic Survey data products from observations made with the ESO Very Large Telescope at the La Silla Paranal Observatory under programme ID 188.B-3002. These data products have been processed by the Cambridge Astronomy Survey Unit (CASU) at the Institute of Astronomy, University of Cambridge, and the FLAMES/UVES reduction team at INAF/Osservatorio Astrofisico di Arcetri. The *Gaia*-ESO Survey Data Archive is prepared and hosted by the Wide Field Astronomy Unit, Institute for Astronomy, University of Edinburgh, which is funded by the UK Science and Technology Facilities Council. The anonymous referee is thanked for helpful suggestions. S.L.M. acknowledges support from the Australian Research Council through grant DP180101791 and from the UNSW Scientia Fellowship program. T.B. was funded by grant No. 2018-04857 from The Swedish Research Council. U.H. acknowledges support from the Swedish National Space Agency (SNSA/Rymdstyrelsen). This research has made use of SIMBAD (operated at CDS, Strasbourg), of VALD (Kupka et al. 2000), and of NASA's Astrophysics Data System. This work has made use of data from the European Space Agency (ESA) mission *Gaia* (https://www.cosmos.esa.int/gaia), processed by the *Gaia* Data Processing and Analysis Consortium (DPAC, https://www.cosmos.esa.int/web/gaia/dpac/consortium). Funding for the DPAC has been provided by national institutions, in particular the institutions participating in the *Gaia* Multilateral Agreement.

References

Aguado, D. S., Belokurov, V., Myeong, G. C., et al. 2021, ApJ, 908, L8
Alves-Brito, A., Yong, D., Meléndez, J., Vásquez, S., & Karakas, A. I. 2012, A&A, 540, A3
Asplund, M. 2004, Mem. Soc. Astron. It., 75, 300
Bastian, N., & Lardo, C. 2018, ARA&A, 56, 83
Bastian, N., Cabrera-Ziri, I., Davies, B., & Larsen, S. S. 2013, MNRAS, 436, 2852
Bastian, N., Cabrera-Ziri, I., & Salaris, M. 2015, MNRAS, 449, 3333
Baumgardt, H., & Hilker, M. 2018, MNRAS, 478, 1520
Bekki, K., & Yong, D. 2012, MNRAS, 419, 2063
Bergemann, M., Hoppe, R., Semenova, E., et al. 2021, MNRAS, 508, 2236
Bressan, A., Marigo, P., Girardi, L., et al. 2012, MNRAS, 427, 127
Busso, M., Wasserburg, G. J., Nollett, K. M., & Calandra, A. 2007, ApJ, 671, 802
Campbell, S. W., Yong, D., Wylie-de Boer, E. C., et al. 2012, ApJ, 761, L2
Cantiello, M., & Langer, N. 2010, A&A, 521, A9
Carretta, E., Gratton, R. G., Lucatello, S., et al. 2010, ApJ, 722, L1
Carretta, E., Lucatello, S., Gratton, R. G., Bragaglia, A., & D'Orazi, V. 2011, A&A, 533, A69
Cassisi, S., Salaris, M., Pietrinferni, A., et al. 2008, ApJ, 672, L115
Chanamé, J., Pinsonneault, M., & Terndrup, D. M. 2005, ApJ, 631, 540
Charbonnel, C., & Lagarde, N. 2010, A&A, 522, A10
Charbonnel, C., & Zahn, J.-P. 2007, A&A, 467, L15
Clegg, R. E. S., Tomkin, J., & Lambert, D. L. 1981, ApJ, 250, 262
de Mink, S. E., Pols, O. R., Langer, N., & Izzard, R. G. 2009, A&A, 507, L1
Dekker, H., D'Odorico, S., Kaufer, A., Delabre, B., & Kotzlowski, H. 2000, in Optical and IR Telescope Instrumentation and Detectors, eds. M. Iye, & A. F. Moorwood, Proc. SPIE, 4008, 534
Denissenkov, P. A., & Tout, C. A. 2000, MNRAS, 316, 395
Denissenkov, P. A., Chaboyer, B., & Li, K. 2006, ApJ, 641, 1087
Denissenkov, P. A., Pinsonneault, M., & MacGregor, K. B. 2009, ApJ, 696, 1823
Dinescu, D. I., Girard, T. M., & van Altena, W. F. 1999, AJ, 117, 1792
Eggenberger, P., Maeder, A., & Meynet, G. 2005, A&A, 440, L9
Eggleton, P. P., Dearborn, D. S. P., & Lattanzio, J. C. 2006, Science, 314, 1580
Eggleton, P. P., Dearborn, D. S. P., & Lattanzio, J. C. 2008, ApJ, 677, 581
Forbes, D. A. 2020, MNRAS, 493, 847
Gaia Collaboration (Prusti, T., et al.) 2016, A&A, 595, A1
Gaia Collaboration (Brown, A. G. A., et al.) 2018, A&A, 616, A1
Gieles, M., Charbonnel, C., Krause, M. G. H., et al. 2018, MNRAS, 478, 2461
Gilmore, G., Randich, S., Asplund, M., et al. 2012, The Messenger, 147, 25
Gratton, R. G., Villanova, S., Lucatello, S., et al. 2012a, A&A, 544, A12
Gratton, R. G., Carretta, E., & Bragaglia, A. 2012b, A&ARv, 20, 50
Gratton, R. G., Lucatello, S., Carretta, E., et al. 2012c, A&A, 539, A19
Gratton, R., Bragaglia, A., Carretta, E., et al. 2019, A&ARv, 27, 8
Grevesse, N., Asplund, M., & Sauval, A. J. 2007, Space Sci. Rev., 130, 105
Grundahl, F., & Bruntt, H. 2006, Chemical Abundances and Mixing in Stars in the Milky Way and its Satellites, 132
Gustafsson, B., Edvardsson, B., Eriksson, K., et al. 2008, A&A, 486, 951
Gustafsson, B., Karlsson, T., Olsson, E., Edvardsson, B., & Ryde, N. 1999, A&A, 342, 426
Harris, W. E. 1996, AJ, 112, 1487
Heiter, U., Jofré, P., Gustafsson, B., et al. 2015, A&A, 582, A49
Heiter, U., Lind, K., Bergemann, M., et al. 2021, A&A, 645, A106
Helmi, A., Babusiaux, C., Koppelman, H. H., et al. 2018, Nature, 563, 85
Hesser, J. E., Bell, R. A., Harris, G. L. H., & Cannon, R. D. 1982, AJ, 87, 1470
Hubbard, E. N., & Dearborn, D. S. P. 1980, ApJ, 239, 248
Jofré, P., Heiter, U., Soubiran, C., et al. 2014, A&A, 564, A133
Johansson, S., Litzén, U., Lundberg, H., & Zhang, Z. 2003, ApJ, 584, L107
Koch-Hansen, A. J., Hansen, C. J., & McWilliam, A. 2021, A&A, 653, A2
Korotin, S. A., Andrievsky, S. M., Luck, R. E., et al. 2014, MNRAS, 444, 3301
Kovalev, M., Bergemann, M., Ting, Y.-S., & Rix, H.-W. 2019, A&A, 628, A54
Kunder, A., Bono, G., Piffl, T., et al. 2014, A&A, 572, A30
Kupka, F. G., Ryabchikova, T. A., Piskunov, N. E., Stempels, H. C., & Weiss, W. W. 2000, Balt. Astron., 9, 590
Kurucz, R. L. 2005, Mem. Soc. Astron. It. Suppl., 8, 189
Kuzma, P. B., Da Costa, G. S., & Mackey, A. D. 2018, MNRAS, 473, 2881
Lagarde, N., Decressin, T., Charbonnel, C., et al. 2012, A&A, 543, A108
Lagarde, N., Reylé, C., Robin, A. C., et al. 2019, A&A, 621, A24
Lardo, C., Milone, A. P., Marino, A. F., et al. 2012, A&A, 541, A141
Lardo, C., Pancino, E., Mucciarelli, A., et al. 2013, MNRAS, 433, 1941
Lee, J.-W. 2016, ApJS, 226, 16
Lee, J.-W. 2020, ApJ, 888, L6
Li, H., Hammer, F., Babusiaux, C., et al. 2021, ApJ, 916, 8
Lim, D., Han, S.-I., Lee, Y.-W., et al. 2015, ApJS, 216, 19
Lind, K., Asplund, M., Barklem, P. S., & Belyaev, A. K. 2011, A&A, 528, A103
Marino, A. F., Sneden, C., Kraft, R. P., et al. 2011, A&A, 532, A8
Marino, A. F., Milone, A. P., Yong, D., et al. 2014, MNRAS, 442, 3044
Massari, D., Koppelman, H. H., & Helmi, A. 2019, A&A, 630, L4
Matsuno, T., Hirai, Y., Tarumi, Y., et al. 2021, A&A, 650, A110
Mészáros, S., Masseron, T., Fernández-Trincado, J. G., et al. 2021, MNRAS, 505, 1645
Milone, A. P., Bedin, L. R., Piotto, G., et al. 2008, ApJ, 673, 241
Monelli, M., Milone, A. P., Stetson, P. B., et al. 2013, MNRAS, 431, 2126
Mucciarelli, A., Lapenna, E., Massari, D., et al. 2015, ApJ, 809, 128
Navin, C. A., Martell, S. L., & Zucker, D. B. 2015, MNRAS, 453, 531
Nordhaus, J., Busso, M., Wasserburg, G. J., Blackman, E. G., & Palmerini, S. 2008, ApJ, 684, L29
Olszewski, E. W., Saha, A., Knezek, P., et al. 2009, AJ, 138, 1570
Pagel, B. E. J., & Tautvaisiene, G. 1995, MNRAS, 276, 505
Pagel, B. E. J., & Tautvaisiene, G. 1997, MNRAS, 288, 108
Pagel, B. E. J., & Tautvaisiene, G. 1998, MNRAS, 299, 535
Palacios, A., Talon, S., Charbonnel, C., & Forestini, M. 2003, A&A, 399, 603
Palmerini, S., Busso, M., Maiorca, E., & Guandalini, R. 2009, PASA, 26, 161
Pancino, E., Rejkuba, M., Zoccali, M., & Carrera, R. 2010, A&A, 524, A44
Pancino, E., Romano, D., Tang, B., et al. 2017a, A&A, 601, A112
Pancino, E., Lardo, C., Altavilla, G., et al. 2017b, A&A, 598, A5
Pasquini, L., Avila, G., Blecha, A., et al. 2002, The Messenger, 110, 1
Pawlowski, M. S., & Kroupa, P. 2013, MNRAS, 435, 2116
Pereira, T. M. D., Kiselman, D., & Asplund, M. 2009, A&A, 507, 417
Plez, B. 2012, Astrophysics Source Code Library [record ascl:1205.004]
Randich, S., & Magrini, L. 2021, Front. Astron. Space Sci., 8, 6
Randich, S., Gilmore, G., & Gaia-ESO Consortium 2013, The Messenger, 154, 47
Ruffoni, M. P., Den Hartog, E. A., Lawler, J. E., et al. 2014, MNRAS, 441, 3127
Sacco, G. G., Morbidelli, L., Franciosini, E., et al. 2014, A&A, 565, A113
Sanna, N., Franciosini, E., Pancino, E., & Mucciarelli, A. 2020, Mem. Soc. Astron. It., 91, 101
Simpson, J. D., Martell, S. L., & Navin, C. A. 2017, MNRAS, 465, 1123
Smiljanic, R., Korn, A. J., Bergemann, M., et al. 2014, A&A, 570, A122
Stetson, P. B., Pancino, E., Zocchi, A., Sanna, N., & Monelli, M. 2019, MNRAS, 485, 3042
Sweigart, A. V., & Mengel, J. G. 1979, ApJ, 229, 624
Tautvaišienė, G., Drazdauskas, A., Mikolaitis, Š., et al. 2015, A&A, 573, A55
Valcin, D., Bernal, J. L., Jimenez, R., Verde, L., & Wandelt, B. D. 2020, JCAP, 2020, 002
van den Bergh, S. 1996, ApJ, 471, L31
Ventura, P., Carini, R., & D'Antona, F. 2011, MNRAS, 415, 3865
Villanova, S., Geisler, D., & Piotto, G. 2010, ApJ, 722, L18
Vincenzo, F., Spitoni, E., Calura, F., et al. 2019, MNRAS, 487, L47
Wang, E. X., Nordlander, T., Asplund, M., et al. 2021, MNRAS, 500, 2159
Yong, D., & Grundahl, F. 2008, ApJ, 672, L29
Yong, D., Grundahl, F., Nissen, P. E., Jensen, H. R., & Lambert, D. L. 2005, A&A, 438, 875
Yong, D., Grundahl, F., D'Antona, F., et al. 2009, ApJ, 695, L62
Yong, D., Grundahl, F., & Norris, J. E. 2015, MNRAS, 446, 3319
Zahn, J.-P., Talon, S., & Matias, J. 1997, A&A, 322, 320

[1] Institute of Theoretical Physics and Astronomy, Vilnius University, Saulėtekio Av. 3, 10257 Vilnius, Lithuania
e-mail: grazina.tautvaisiene@tfai.vu.lt

[2] INAF – Osservatorio di Astrofisica e Scienza dello Spazio, Via Gobetti 93/3, 40129 Bologna, Italy
[3] Department of Astrophysics, School of Physics, University of New South Wales, Sydney, NSW 2052, Australia
[4] UNSW Data Science Hub, University of New South Wales, Sydney, NSW 2052, Australia
[5] INAF – Osservatorio Astrofisico di Arcetri, Largo Enrico Fermi 5, 50125 Firenze, Italy
[6] Space Science Data Center, Via del Politecnico SNC, 00133 Roma, Italy
[7] Dipartimento di Fisica e Astronomia, Università degli Studi di Bologna, Via Gobetti 93/2, 40129 Bologna, Italy
[8] Nicolaus Copernicus Astronomical Center, Polish Academy of Sciences, ul. Bartycka 18, 00-716 Warsaw, Poland
[9] Institute of Astronomy, University of Cambridge, Madingley Road, Cambridge CB3 0HA, UK
[10] Lund Observatory, Department of Astronomy and Theoretical Physics, Box 43, 221 00 Lund, Sweden
[11] Max-Planck Institut für Astronomie, Königstuhl 17, 69117 Heidelberg, Germany
[12] Leibniz-Institut für Astrophysik Potsdam, An der Sternwarte 16, 14482 Potsdam, Germany
[13] Dipartimento di Fisica e Astronomia, Università di Padova, Vicolo Osservatorio 3, 35122 Padova, Italy
[14] Observational Astrophysics, Department of Physics and Astronomy, Uppsala University, Box 516, 75120 Uppsala, Sweden
[15] INAF – Osservatorio Astronomico di Padova, Vicolo dell'Osservatorio, 5, 35122 Padova, Italy